Agastache rugosa alleviates the multi-hit effect on hepatic lipid metabolism, inflammation and oxidative stress during nonalcoholic fatty liver disease

Yizhe Cui
Heilongjiang Bayi Agricultural University https://orcid.org/0000-0002-7877-8328
Renxu Chang
Heilongjiang Bayi Agricultural University
Qiuju Wang
Heilongjiang Bayi Agricultural University
Yusheng Liang
University of Illinois at Urbana-Champaign
Juan J Loor
University of Illinois at Urbana-Champaign
Chuang Xu (xuchuang7175@163.com)
Heilongjiang Bayi Agricultural University

Research

Keywords: NAFLD, Agastache rugosa, mice, AML12 cells, multi-targets

Posted Date: April 21st, 2020

DOI: https://doi.org/10.21203/rs.3.rs-21957/v1

Abstract

Background

Non-alcoholic fatty liver disease (NAFLD) is the most common cause of chronic liver disease, and has high rates of morbidity and mortality worldwide. *Agastache rugosa* (AR) possesses unique anti-oxidant, anti-inflammatory and anti-atherosclerosis characteristics.

Methods

To investigate the effects and the underlying mechanism of AR on NAFLD, we fed mice a high-fat diet (HFD) to establish NAFLD model of mice in vivo experiment and induced lipidosis in AML12 hepatocytes through a challenge with free fatty acids (FFA) in vitro. The contents of total cholesterol (TC), triglyceride (TG), alanine aminotransferase (ALT) and aspartate aminotransferase (AST) in liver homogenates were measured. Pathological changes in liver tissue were evaluated by HE staining. Oil red O staining was used to determine degree of lipid accumulation in liver tissue, and Western blot was used to detect abundance of inflammation-, lipid metabolism- and endoplasmic reticulum stress-related proteins.

Results

Supply of AR alleviated accumulation of lipid in hepatocytes induced by HFD in vivo and challenged with free fatty acids (FFA) in vitro. Compared with the HFD group, supplementing AR decreased p-NF-κB/NF-κB and p-IκB/IκB protein and inhibited abundance of PERK, IRE1 and ATF6 ($P < 0.05$). Furthermore, AR reduced lipid accumulation within hepatocytes by downregulating abundance of SREBP, ACC1 and FAS ($P < 0.05$). Supply of AR significantly attenuated ROS accumulation and MDA production by improving antioxidant enzymatic activity including SOD and GSH ($P < 0.01$).

Conclusion

Supply of AR attenuates disordered lipid metabolism and enhances the antioxidative defense associated with NAFLD induced by HFD in mice. Results underscore the potential of plants used in traditional Chinese medicine to achieve pharmacological benefits through a multi-tier cellular response.

Introduction

Nonalcoholic fatty liver disease (NAFLD) is an important component of the metabolic syndrome in states such as obesity and insulin resistance [1]. Inflammatory reactions induced by reactive oxygen species in the liver parenchymal cells characterize the so-called “first-hit” during NAFLD [2]. Dysregulation of adipocyte metabolism in the metabolic syndrome is an independent risk factor for development of NAFLD [3]. Natural substances are not only effective treatment for obesity, diabetes, insulin resistance

(IR) and other metabolic diseases, but also relatively safe to consume [4]. Traditional Chinese medicine (TCM) formulas based on plant extracts contain substances capable of eliciting the so-called "multiple organ-multiple hit" effect [5]. Various TCM and supplements offer suitable therapeutic options in the treatment and prevention of NAFLD [6]. For instance, *Agastache rugosa* (AR), a herbal drug, has been used in humans for the treatment of anorexia, vomiting and other intestinal disorders [7, 8]. Studies indicate that AR has anticarcinogenic [9] and protective effects against lung [10] and brain injury [11]. Extracts of AR are also believed to be valuable in the treatment of inflammatory [12] and oxidative stress-induced disorders [13]. Therefore, our general hypothesis was that supply of AR would attenuate the negative effects of NAFLD on hepatic lipid metabolism and oxidative stress. At present, the effect of *Agastache rugosa* on NAFLD is unknown. Thus, specific objectives were to induce NAFLD in vivo and in vitro to study the underlying mechanisms whereby supply of AR can have a positive effect.

Materials And Methods

Herbal plant extract

AR was purchased from Daqing Fu Rui Bang pharmacy, China. The raw herbs were soaked in distilled water overnight followed by decocting twice in boiling water (60 min each time). The combined aqueous extract was filtered through gauze and then heated until evaporation [14]. Insoluble particles were removed by low-speed centrifugation, the supernatant sterilized by filtration through a 0.22 μm Millipore filter (MILLEX, GP) and stored at 4 °C for use. Main components of AR were analyzed by high-performance liquid chromatography-electrospray ionization/mass spectrometry (LC/MS).

Animals and treatment

Male Kun Ming mice (20–22 g; 8 weeks) were obtained from Harbin Medical University (Daqing, China). Mice were housed in cages with a 12 h light/dark cycle in a temperature-controlled environment. The mice were acclimatized to laboratory conditions for 1 week before the study and then randomly divided into five groups of six: control group fed a standard diet, NAFLD group fed a high fat diet (HFD) (60% kcal fat), low dose group fed HFD + 1.8 g/kg AR given orally (0.1 mL per 10 g body weight), medium dose group (HFD + 4.5 g/kg AR) and high dose group (HFD + 9.0 g/kg AR). HFD feeding was initiated at 8 weeks of age and continued for an additional 8 weeks at which point mice were fasted for 12 h prior to sacrifice with ether. Blood was collected just before sacrifice for serum biochemical analysis. The liver was quickly excised, cleaned completely with ice-cold phosphate-buffered saline (PBS), weighed and preserved in liquid nitrogen until use. All animal studies were approved by the Ethics Committee of Heilongjiang Bayi Agricultural University in accordance with the Chinese guidelines for the care and use of laboratory animals.

Histological Examination

A portion of liver tissue was fixed with 4% paraformaldehyde and embedded in paraffin. For hematoxylin and eosin (H&E) staining [15], rehydration was done in a decreasing ethanol series, and then stained with

H&E. Frozen sections were prepared and stained with Oil red O to determine hepatic lipid accumulation. The most severe areas with hepatic inflammation in the representative histology sections were photographed using a microscope. Cells were fixed with 4% paraformaldehyde and stained with freshly diluted Oil Red O solution. Representative photomicrographs were captured using a system incorporated in the microscope.

ELISA assays

To detect liver biochemical indicators, tissue was first placed in pre-cooled PBS and ground into a homogenate, followed by centrifugation to recover the supernatant for analyses. Determination of alanine aminotransferase (ALT) (Catalog No. BPE20168), aspartate aminotransferase (AST) (Catalog No. BPE20184), tumor necrosis factor-α (TNF-α) (Catalog No. BPE20220), interleukin-6 (IL-6) (Catalog No. BPE20012), malondialdehyde (MDA) (Catalog No. BPE20347), glutathione (GSH) (Catalog No. BPE20879), superoxide dismutase (SOD) (Catalog No. BPE20348), triglyceride (TG) (Catalog No. BPE20754) and total cholesterol (TC) (Catalog No. BPE20095) were quantified via ELISA (Shanghai Lengton Bioscience Co.,LTD) (ShangHai, China). All assays were performed according to the manufacturer's instructions.

Cell culture

Alpha mouse liver 12 (AML12) cells, a hepatocyte cell line from a mouse transgenic for human transforming growth factor α, were kindly provided by Stem Cell Bank, Chinese Academy of Sciences and cultured in the manufacturer's recommended medium composed of DMEM-F12 (gibco, 12400-024) medium containing 10% fetal bovine serum (CLARK, FB25015), 1% streptomycin (100 μg/mL) and penicillin–streptomycin (100 U/mL) (Solarbio, P1400), 1% transferrin (gibco, 41400-045), and 40 ng/mL dexamethasone (SIGMA, D4902-25MG). Cells were incubated with fresh medium at 37 °C in 95% air, 5% CO_2, and used in each experiment after 3 days.

Cell viability analysis

3-(4,5-dimethyl-2-thiazolyl)-2,5-diphenyl-2-H-tetrazolium bromide (MTT) (Solarbio, M8180) was used to analyze cell viability. Cells were treated with different concentrations of AR for 20 h, and then 10 μL MTT was added for another 4 h. Culture medium was then totally removed and DMSO added, followed by measurement of absorbance using a microplate reader. All MTT assays were performed at least 3 times for each group. Subsequently, results of the MTT assay were used to select 5 different concentrations of AR to add to cell culture fluid. Real-time cell growth curves were measured through the Real-time label-free cell analysis (RTCA) system (ACEA Biosciences).

Cell treatment

AML12 cells were seeded in 6-well plates. Hepatic steatosis in vitro was induced according to previously established methods [16] in which AML12 cells were treated for 24 h with a mixture of FFA containing a 2:1 ratio of oleate (SIGMA, O1383-5G) and palmitate (SIGMA, P5585-10G), the final concentration of FFA being 1 mM. For the AR supplementation experiment, the herbal extracts were added to the above

medium containing 1 mM FFA for 24 h at a high (25 mg/mL), medium (12.5 mg/mL), or low (6.25 mg/mL) concentration.

Protein extraction and Western blotting

Liver or AML12 cell samples were prepared to lysates containing protease inhibitors by adding frozen RIPA buffer before determining protein concentration with the BCA kit (Beyotime, P0010). Protein samples (25 μg) were separated on 10% Bis–Tris SDS-PAGE gel and then transferred onto PVDF membranes. After blocking for 1 hour in a TBST (0.1% Tween 20, pH 7.4) with 5% nonfat milk, the membranes were incubated overnight with the indicated primary antibodies. After dilution with TBST (1:1000 dilution), ACC1 (abcam, ab45174), FAS (CST, 3180S), SREBP1 (NOVUSBIO, NB100-2215), NF-κB (CST, 6956S), p-NF-κB (CST, 3033S), IκBα (CST, 4814S), p-IκBα (CST, 2859S), IKKα (CST, 2682S), ATF6 (abcam, ab203119), PERK (CST, 3192S), IRE1 (abcam,ab37073), monoclonal antibody was used to detect protein expression levels in the samples. Membranes were washed 3x with TBST, followed by a 30-min room temperature incubation with HRP labeled goat antimouse or goat anti rabbit (3:5000; Beyotime, A0208, A0216) in TBST plus 5% milk. Membranes were washed as before and then developed using HaiGene (M2301) detection kit and imaged with AI600. ImageJ software was used to detect protein abundance.

Confocal laser fluorescence imaging

For immunofluorescence [17], cells were plated on coverslips at a density of 0.5×10^5 cells per well followed by treatment, and fixed with 4% paraformaldehyde for 30 min. After incubating in blocking solution (3% Bovine Serum Albumin, 5% Goat serum, 0.5% Triton 100 in PBS, pH 7.4) for 30 min, cells were incubated overnight in 4 ℃ with NF-κB (1:800) antibody. Cells were then washed with PBS 5 times and incubated with FITC conjugated goat anti-mouse IgG (E1216, Santa Cruz Blotechnology) for 1 h. Hochest 33342 (C1026, Beyotime) was used for nuclear staining. Fluorescence images were observed and photographed by using an immunofluorescence microscope (Leica microsystems).

Flow cytometry

To measure the production of ROS, we employed the Reactive Oxygen Species Assay Kit (APPLYGEN, C1300) according to the manufacturer's instructions. Results were then analyzed by fluorescent microscopy and a flow cytometer (BD Biosciences, USA) [18].

Statistical analysis

All results are expressed as the mean ± SD. Statistical analyses were performed using the Student t-test. For multiple comparisons, one-way analysis of variance (ANOVA) was used. $P < 0.05$ was considered statistically significant.

Results

AR alleviated liver lesions induced by HFD

Compared with the control group, the content of ALT and AST in the liver homogenate of the HFD group increased significantly ($P < 0.01$); compared with the HFD group, the content of ALT and AST in the AR group decreased with the increase of AR concentration (Fig. 1A).

The structure of hepatocytes based on HE staining indicated that the control group had complete structural features, i.e. hepatocytes were polygonal, boundary was clear, cytoplasm stained red, there were no vacuoles, the nucleus was in the center; the outline of liver lobules was clear, the structure was regular, and the liver cords were arranged radially with the central vein as the axis. However, in the HFD group, there were diffuse vacuoles around the central vein and portal area, the boundary between the cells in the field of vision was unclear, hepatocytes were obviously swollen or inflated like balloons, a large number of nearly round vacuoles could be seen in the cells, even the vacuoles squeezed the nucleus of the liver to one side; the hepatic sinuses were compressed and narrow, and the structures of the hepatic sinuses and hepatic cords were unclear. Compared with the HFD group, liver tissue of the AR group was improved in terms of hepatic sinuses, structural arrangement of hepatic cords, morphology of liver cells, and fat globules and balloon like changes (Fig. 1B).

Changes of oil red O staining in liver tissue showed that the nucleus in the control group was blue, there were no obvious orange lipid droplets, space between liver cells was clear, and the structure of liver sinuses was normal. In the HFD group, however, hepatocytes were enlarged with diffused lipid droplets in the field of vision. In contrast, in the AR group the content of orange lipid droplets was significantly lower than the HFD group, and there was a reduction in lipid accumulation (Fig. 1B).

In the FFA group, oil red O staining showed a large number of lipid droplets in AML12 cells, and some of the fusion showed chain and mass changes. In the AR group, the number of orange lipid droplets in hepatocytes was significantly lower than the model group, and the degree of lipid accumulation was reduced which was consistent with the change observed in liver tissue (Fig. 1C).

AR increased liver antioxidant capacity during NAFLD induced by HFD

Compared with the control group, the activity of SOD and GSH in the liver of HFD group decreased significantly ($P < 0.01$), while MDA increased significantly ($P < 0.01$). Furthermore, AR significantly increased GSH level ($P < 0.01$) and decreased MDA level ($P < 0.01$) in a dose-dependent manner (Fig. 2A). In AML12 cells, the content of ROS in the FFA group was significantly greater ($P < 0.01$) than the control group, while content of ROS in the AR groups was significantly lower ($P < 0.01$) than the control group (Fig. 2B).

AR suppresses inflammation in liver and AML12 cells

Compared with the control group, the levels of TNF-α,IL-6 and abundance of IKK, p-NF-κB/NF-κB and p-IκB/IκB protein in the liver of HFD group increased significantly ($P < 0.01$), while they decreased significantly ($P < 0.01$) in the 9.0 g/kg AR group (Fig. 3). Furthermore, AR significantly decreased p-NF-κB/NF-κB and p-IκB/IκB abundance in AML12 cells ($P < 0.01$) (Fig. 4A and B). In AML12 cells, compared with the control group, abundance of NF-κB protein was mainly distributed in the nucleus of the FFA group, while abundance of NF-κB protein increased in the cytoplasm of the AR group (Fig. 4C).

AR reduced fat deposition during NAFLD induced by HFD

Compared with the control group, the content of TC and TG in liver homogenate of the HFD group was significantly increased ($P < 0.01$); compared with the HFD group, the content of TC and TG in liver homogenate of the AR group was significantly lower ($P < 0.01$) (Fig. 5A). In addition, compared with the control group, abundance of SREBP, ACC1 and FAS were significantly upregulated in the HFD group. Compared with the HFD group, the AR group significantly decreased abundance of SREBP, ACC1 and FAS (Fig. 5B). In addition, protein abundance of SREBP and FAS decreased in a dose-dependent manner in the AR groups. Furthermore, the abundance trend of SREBP, ACC1 and FAS in AML12 cells was consistent with that in liver tissue (Fig. 5C).

AR alleviated ER stress during NAFLD induced by HFD

Protein abundance of PERK, IRE1 and ATF6 in liver of the HFD group was increased significantly compared to the normal group ($P < 0.05$). No difference was observed in the different dose groups of AR ($P > 0.05$), whereas marked decrease in abundance of PERK, IRE1 and ATF6 was observed in the AR group compared with the HFD group ($P < 0.05$) (Fig. 6A). Compared with the control cells, cells treated with FFA showed significantly increased levels of PERK and IRE1 ($P < 0.05$). Compared with FFA-treated cells, cells pretreated with AR showed significantly lowered protein abundance of PERK and IRE1 ($P < 0.05$) in a dose-dependent manner (Fig. 6B).

Compositions of compounds in the AR

The chemical composition of AR of peak MS spectrum of was showed in Fig. 7. The concentrations of substances were showed in Table 1 and Table 2. Ninety-nine compounds were identified where the concentration of flavonoids was 33%. The full spectrums of constituents were identified based on the database Metlin (https://metlin.scripps.edu).

Discussion

The hallmark of NAFLD is the hepatic accumulation of lipids, which subsequently leads to cellular stress, inflammation and hepatic injury, eventually resulting in chronic liver disease [19, 20]. Abnormal lipid accumulation often coincides with insulin resistance in steatotic livers and is associated with perturbed endoplasmic reticulum (ER) proteostasis in hepatocytes [21]. The main components of AR are terpenoids, ketones, alcohols, aldehydes and flavonoids [22]. Flavonoids have many pharmacological effects, such as anti-oxidation, anti-inflammatory, analgesic, immunomodulatory, anti-aging, hypolipidemic, anti-tumor, etc [23]. Our results show that AR can reduce lipid accumulation, anti-inflammatory and enhance antioxidant capacity.

Oxidative stress is a key factor of the "second hit" theory during NAFLD [24]. Accumulation of lipid in hepatocytes leads to acceleration of mitochondrial β oxidation capacity to compensate, which in turn enhances production of ROS that often exceeds the antioxidant capacity of liver and causes oxidative stress [25]. Studies found that the serum SOD and GSH decreased while MDA increased significantly in NAFLD [26]. The antioxidant effect of AR was dose-dependent and led to increased HO-1 protein and enzyme activity, and protected cells from H_2O_2-induced cytotoxicity [27]. Such response also attenuated

UVB-induced photoaging by upregulating anti-oxidant enzymes [28] and reducing the production of ROS [29]. Our results showed that compared with the HFD group, the levels of SOD and GSH in the liver of AR group were significantly increased, while the levels of MDA and ROS were significantly decreased in hepatocytes (Fig. 2). Thus, we speculate that AR decreased lipid peroxidation directly through increasing antioxidant enzymes activites.

An HFD increase in mitochondrial β oxidation can cause oxidative stress, and the increase of ROS production can activate the inflammatory pathway regulated by IKK/NF-κB [30]. As a prototypical component of a proinflammatory signaling pathway, NF-κB induces the transcription of numerous proinflammatory cytokines (TNF- α and IL-6) [31]. In terms of anti-inflammatory effects, essential oils in AR suppressed nitric oxide (NO) production by inactivating NF-κB in lipopolysaccharide (LPS)-stimulated RAW264.7 cells [32]. AR prevented the activation and translocation of NF-κB to the nucleus from the cytosol fraction [33, 34]. Our study showed that AR not only decreased NF-κB-induced transcription of inflammatory cytokines in HFD-induced NAFLD (Fig. 3A), but also inhibited protein abundance of IKK-NF-κB signaling pathway components (Fig. 3 and Fig. 4). These results suggest that AR might inhibit activation of IKK/IKB/NF-κB signaling to interrupt the inflammatory cascade, and reduce the "second hit" of inflammatory factors on liver.

Serum enzymology and blood lipid are typical indices used for clinical diagnosis of NAFLD, but liver histology is still the "gold standard" [35]. Our results showed that compared with the HFD group, the AR group reduced TC and TG (Fig. 5A), and the AR group reduced lipid accumulation in hepatocytes (Fig. 1). HFD can lead to hyperlipidemia and disorders of liver lipid metabolism including accumulation of TG in liver [31] and liver cell degeneration. According to the pathogenesis of HFD-induced NAFLD, many natural products can regulate hepatic lipogenesis and esterification of fatty acids into TG [36]. SREBP is a key regulator of lipogenesis, and over-activation of this process is one characteristic of NAFLD [37]. Hence, down-regulation of ACC and FAS could prevent NAFLD [38]. Recent studies reported that extracts from AR had anti-adipogenic effects in 3T3-L1 adipocytes [39]. Thus, our results indicating that AR decreased abundance of SREBP, ACC1 and FAS to modulate lipid accumulation and attenuate NAFLD induced by HFD suggest that it is a potent anti-lipogenic compound.

Endoplasmic reticulum (ER) stress has been identified as a crucial feature of NAFLD [40]. ER is the major organelle for properly folding and post-translational modifications of proteins and acts as a major intracellular calcium reservoir in the cell. High-fat diets activate ER stress in liver [25] with PERK, IRE1 and ATF6 being involved in the development of NAFLD [41]. The unfolded protein response (UPR) is a complementary adaptive machinery against ER stress, and is coordinated by three ER transmembrane receptor proteins; Inositol requiring kinase 1 (IRE1), double-stranded RNA-activated protein kinase (PKR)-like endoplasmic reticulum kinase (PERK) and activating transcription factor 6 (ATF6) [42]. We found that AR alleviated hepatic steatosis by decreasing ERS-related protein expression in vivo and in vitro models. This confirms the suggestion of Sandoval IV [43] who concluded that AR could be successful in preventing ER stress.

Conclusion

Our studies suggested that AR could alleviate hepatic inflammation, steatosis and oxidative stress in in vivo an in vitro models of NAFLD. The data provide the basis for developing novel bioactive food additives based on AR that can help alleviate complications associated with development of NAFLD.

Abbreviations

NAFLD: Non-alcoholic fatty liver disease; IR: insulin resistance; TCM: Traditional Chinese medicine; AR: *Agastache rugosa*; LC/MS: liquid chromatography-electrospray ionization/mass spectrometry; H&E: hematoxylin and eosin; AML12: Alpha mouse liver 12; MTT: 3-(4,5-dimethyl-2-thiazolyl)-2,5-diphenyl-2-H-tetrazolium bromide; TC: total cholesterol; TG: triglyceride; ALT: alanine aminotransferase; AST: aspartate aminotransferase; HFD: high-fat diet; FFA: free fatty acid; TNF-α: tumor necrosis factor-α; IL-6: interleukin-6; MDA: malondialdehyde; GSH: glutathione; SOD: superoxide dismutase; NF-κB: nuclear factor-κB; IKK: inhibitor of KappaB kinase; IκB: inhibitor of NF-κB; SREBP: sterol regulatory element binding protein; ACC1: acetyl-CoA carboxylase 1; FAS: fatty acid synthase; ATF6: activating transcription factor 6; IRE1: inositol-requiring enzyme-1; PERK: protein kinase (PKR)-like endoplasmic reticulum kinase.

Declarations

Ethics approval and consent to participate

All the experimental procedures were approved by, and conducted in accordance with Principles of Laboratory Animal Care and according to the rules and ethics set forth by the Ethical Committee of Heilongjiang Bayi Agricultural University.

Consent for publication

Not applicable.

Availability of data and materials

All the data obtained and materials analyzed in this research are available with the corresponding author.

Competing interests

The authors declare that they have no competing interests

Funding

The work was supported in part by the National Key R&D Program of China (2017YFD0502200); Group control technology and product development and demonstration of important mass production disease groups in dairy cattle (GA16B20); Heilongjiang Bayi Agricultural University Support Program for San Heng San Zong (ZRCLG201904).

Authors' Contribution

YC and RC designed, performed sample preparation and data analysis. YC wrote the manuscript. QW participated in the method development and validation. JJ, YL and CX participated in its design and coordination and helped to draft the manuscript. All authors read and approved the final manuscript.

Acknowledgements

Not Applicable.

References

1. Byrne CD, Targher G. NAFLD: a multisystem disease. Journal of hepatology. 2015;62:47–64.
2. Buzzetti E, Pinzani M, Tsochatzis EA. The multiple-hit pathogenesis of non-alcoholic fatty liver disease (NAFLD). Metab Clin Exp. 2016;65:1038–48.
3. Eslam M, George J. (2019) Refining the role of epicardial adipose tissue in non-alcoholic fatty liver disease. Hepatology international.
4. Li J, Ding L, Song B, et al. Emodin improves lipid and glucose metabolism in high fat diet-induced obese mice through regulating SREBP pathway. Eur J Pharmacol. 2016;770:99–109.
5. Yan T, Yan N, Wang P, et al. Herbal drug discovery for the treatment of nonalcoholic fatty liver disease. Acta pharmaceutica Sinica B. 2020;10:3–18.
6. Perumpail BJ, Li AA, Iqbal U, et al. (2018) Potential Therapeutic Benefits of Herbs and Supplements in Patients with NAFLD. Diseases 6.
7. Li HQ, Liu QZ, Liu ZL, Du SS, Deng ZW. Chemical composition and nematicidal activity of essential oil of Agastache rugosa against Meloidogyne incognita. Molecules. 2013;18:4170–80.
8. Tuan PA, Park WT, Xu H, Park NI, Park SU. Accumulation of tilianin and rosmarinic acid and expression of phenylpropanoid biosynthetic genes in Agastache rugosa. J Agric Food Chem. 2012;60:5945–51.
9. Lu X, Yang L, Lu C, et al. (2016) Molecular Role of EGFR-MAPK Pathway in Patchouli Alcohol-Induced Apoptosis and Cell Cycle Arrest on A549 Cells In Vitro and In Vivo. BioMed research international 2016: 4567580.
10. Su Z, Liao J, Liu Y, et al. Protective effects of patchouli alcohol isolated from Pogostemon cablin on lipopolysaccharide-induced acute lung injury in mice. Experimental therapeutic medicine. 2016;11:674–82.
11. Wei LL, Chen Y, Yu QY, Wang Y, Liu G. Patchouli alcohol protects against ischemia/reperfusion-induced brain injury via inhibiting neuroinflammation in normal and obese mice. Brain research. 2018;1682:61–70.
12. Li YC, Xian YF, Ip SP, et al. Anti-inflammatory activity of patchouli alcohol isolated from Pogostemonis Herba in animal models. Fitoterapia. 2011;82:1295–301.

13. Lian DW, Xu YF, Ren WK, et al. Unraveling the Novel Protective Effect of Patchouli Alcohol Against Helicobacter pylori-Induced Gastritis: Insights Into the Molecular Mechanism in vitro and in vivo. Front Pharmacol. 2018;9:1347.
14. Gou XJ, Feng Q, Fan LL, Zhu J, Hu YY. (2017) Serum and Liver Tissue Metabonomic Study on Fatty Liver in Rats Induced by High-Fat Diet and Intervention Effects of Traditional Chinese Medicine Qushi Huayu Decoction. Evidence-based complementary and alternative medicine: eCAM 2017: 6242697.
15. Ohtani N, Imamura Y, Yamakoshi K, et al. Visualizing the dynamics of p21(Waf1/Cip1) cyclin-dependent kinase inhibitor expression in living animals. Proc Natl Acad Sci USA. 2007;104:15034–9.
16. Zhang X, Yang J, Guo Y, et al. Functional proteomic analysis of nonalcoholic fatty liver disease in rat models: enoyl-coenzyme a hydratase down-regulation exacerbates hepatic steatosis. Hepatology. 2010;51:1190–9.
17. Kim JY, Garcia-Carbonell R, Yamachika S, et al. ER Stress Drives Lipogenesis and Steatohepatitis via Caspase-2 Activation of S1P. Cell. 2018;175:133–45. e115.
18. Cui Y, Chang R, Zhang T, et al. Chinese Herbal Formula (CHF03) Attenuates Non-Alcoholic Fatty Liver Disease (NAFLD) Through Inhibiting Lipogenesis and Anti-Oxidation Mechanisms. Front Pharmacol. 2019;10:1190.
19. Spahis S, Delvin E, Borys JM, Levy E. Oxidative Stress as a Critical Factor in Nonalcoholic Fatty Liver Disease Pathogenesis. Antioxid Redox Signal. 2017;26:519–41.
20. Dalekos GN, Gatselis NK, Zachou K, Koukoulis GK. (2020) NAFLD and autoimmune hepatitis: Do not judge a book by its cover. European journal of internal medicine.
21. Kitade H, Chen G, Ni Y, Ota T. (2017) Nonalcoholic Fatty Liver Disease and Insulin Resistance: New Insights and Potential New Treatments. Nutrients 9.
22. Yamani H, Mantri N, Morrison PD, Pang E. Analysis of the volatile organic compounds from leaves, flower spikes, and nectar of Australian grown Agastache rugosa. BMC Complement Altern Med. 2014;14:495.
23. Lei Z, Sumner BW, Bhatia A, Sarma SJ, Sumner LW. UHPLC-MS Analyses of Plant Flavonoids. Current protocols in plant biology. 2019;4:e20085.
24. Borrelli A, Bonelli P, Tuccillo FM, et al. Role of gut microbiota and oxidative stress in the progression of non-alcoholic fatty liver disease to hepatocarcinoma: Current and innovative therapeutic approaches. Redox Biol. 2018;15:467–79.
25. Hwang I, Uddin MJ, Pak ES, et al. The impaired redox balance in peroxisomes of catalase knockout mice accelerates nonalcoholic fatty liver disease through endoplasmic reticulum stress. Free Radic Biol Med. 2020;148:22–32.
26. Swiderska M, Maciejczyk M, Zalewska A, Pogorzelska J, Flisiak R, Chabowski A. Oxidative stress biomarkers in the serum and plasma of patients with non-alcoholic fatty liver disease (NAFLD). Can plasma AGE be a marker of NAFLD? Oxidative stress biomarkers in NAFLD patients. Free Radic Res. 2019;53:841–50.

27. Oh HM, Kang YJ, Lee YS, et al. Protein kinase G-dependent heme oxygenase-1 induction by Agastache rugosa leaf extract protects RAW264.7 cells from hydrogen peroxide-induced injury. J Ethnopharmacol. 2006;103:229–35.
28. Oh Y, Lim HW, Huang YH, et al. Attenuating properties of Agastache rugosa leaf extract against ultraviolet-B-induced photoaging via up-regulating glutathione and superoxide dismutase in a human keratinocyte cell line. Journal of photochemistry photobiology B Biology. 2016;163:170–6.
29. Shin D, Lee Y, Huang YH, et al. Probiotic fermentation augments the skin anti-photoaging properties of Agastache rugosa through up-regulating antioxidant components in UV-B-irradiated HaCaT keratinocytes. BMC Complement Altern Med. 2018;18:196.
30. de Meneses Fujii TM, Jacob PS, Yamada M, et al. Yerba Mate (Ilex paraguariensis) modulates NF-kappaB pathway and AKT expression in the liver of rats fed on a high-fat diet. Int J Food Sci Nutr. 2014;65:967–76.
31. Cortez M, Carmo LS, Rogero MM, Borelli P, Fock RA. A high-fat diet increases IL-1, IL-6, and TNF-alpha production by increasing NF-kappaB and attenuating PPAR-gamma expression in bone marrow mesenchymal stem cells. Inflammation. 2013;36:379–86.
32. Lee SM, Park KH, Kim SS, Kwon DW, Hong SC. Effect of the Mn oxidation state and lattice oxygen in Mn-based TiO2 catalysts on the low-temperature selective catalytic reduction of NO by NH3. J Air Waste Manag Assoc. 2012;62:1085–92.
33. Oh HM, Kang YJ, Kim SH, et al. Agastache rugosa leaf extract inhibits the iNOS expression in ROS 17/2.8 cells activated with TNF-alpha and IL-1beta. Arch Pharm Res. 2005;28:305–10.
34. Hong JJ, Choi JH, Oh SR, et al. Inhibition of cytokine-induced vascular cell adhesion molecule-1 expression; possible mechanism for anti-atherogenic effect of Agastache rugosa. FEBS Lett. 2001;495:142–7.
35. Castera L, Friedrich-Rust M, Loomba R. Noninvasive Assessment of Liver Disease in Patients With Nonalcoholic Fatty Liver Disease. Gastroenterology. 2019;156:1264–81. e1264.
36. Park YH, Lee JJ, Son HK, Kim BH, Byun J, Ha JH. (2020) Antiobesity Effects of Extract from Spergularia marina Griseb in Adipocytes and High-Fat Diet-Induced Obese Rats. Nutrients 12.
37. Khaleel EF, Abdel-Aleem GA, Mostafa DG. Resveratrol improves high-fat diet induced fatty liver and insulin resistance by concomitantly inhibiting proteolytic cleavage of sterol regulatory element-binding proteins, free fatty acid oxidation, and intestinal triglyceride absorption. Can J Physiol Pharmacol. 2018;96:145–57.
38. Cui CX, Deng JN, Yan L, et al. Silibinin Capsules improves high fat diet-induced nonalcoholic fatty liver disease in hamsters through modifying hepatic de novo lipogenesis and fatty acid oxidation. J Ethnopharmacol. 2017;208:24–35.
39. Park MJ, Song JH, Shon MS, et al. Anti-Adipogenic Effects of Ethanol Extracts Prepared from Selected Medicinal Herbs in 3T3-L1 Cells. Preventive nutrition food science. 2016;21:227–35.
40. Ding S, Jiang J, Zhang G, Bu Y, Zhang G, Zhao X. Resveratrol and caloric restriction prevent hepatic steatosis by regulating SIRT1-autophagy pathway and alleviating endoplasmic reticulum stress in

high-fat diet-fed rats. PloS one. 2017;12:e0183541.

41. Cao J, Dai DL, Yao L, et al. Saturated fatty acid induction of endoplasmic reticulum stress and apoptosis in human liver cells via the PERK/ATF4/CHOP signaling pathway. Molecular cellular biochemistry. 2012;364:115–29.
42. Wang L, Chen J, Ning C, Lei D, Ren J. Endoplasmic Reticulum Stress Related Molecular Mechanisms in Nonalcoholic Fatty Liver Disease (NAFLD). Curr Drug Targets. 2018;19:1087–94.
43. Sandoval IV, Carrasco L. Poliovirus infection and expression of the poliovirus protein 2B provoke the disassembly of the Golgi complex, the organelle target for the antipoliovirus drug Ro-090179. Journal of virology. 1997;71:4679–93.

Tables

Table 1 Chemical components identified from AR by high-performance liquid chromatography-electrospray ionization/mass spectrometry (ESI +)

Name	Rt [min]	Molecular Weight	CAS	Content (ng/μL)
L-Phenylalanine	2.983	165.0785	63-91-2	20.55
L-Arginine	1.201	174.111	74-79-3	6.54
L-Tyrosine	1.397	181.0732	60-18-4	0.26
L-Glutamate	1.313	147.0525	56-86-0	0.18
L-Isoleucine	2.072	131.0941	61-90-5	29.93
L-Lysine	1.16	146.1049	56-87-1	0.35
L-Proline	1.341	115.0628	147-85-3	2.27
Pyroglutamic acid	1.98	129.042	98-79-3	8.26
ferulic acid	4.69	194.0573	1135-24-6	14.81
Sinapic acid	4.66	224.0675	530-59-6	0.83
Styrene	6.038	104.0621	100-42-5	0.10
Chorismic acid	3.906	226.0474	617-12-9	0.03
m-Coumaric acid	4.64	164.0467	588-30-7	2.13
1,2,3-Trihydroxybenzene	3.232	126.0311	533-73-3	1.47
Caffeic Acid	4.48	180.0415	4607-41-4	3.61
Thymol	4.451	150.1038	89-83-8	0.71
Adenosine	1.965	267.0958	58-61-7	3.88
Adenine	1.957	135.0546	73-24-5	0.01
Guanosine	1.96	283.0908	118-00-3	1.44
Guanine	1.441	151.0487	73-40-5	1.96
cAMP	1.473	329.0502	60-92-4	6.56
Quercetin 3-galactoside	4.491	464.0946	482-36-0	0.06
Arcapillin	5.282	360.0832	NA	0.21
Glyceollin	5.928	338.1144	NA	0.01
Isorhamnetin	4.954	316.0571	480-19-3	0.20
Malvidin	5.267	330.0727	643-84-5	0.04
Naringenin	5.177	272.0675	480-41-1	0.06
Quercetin	4.988	302.0415	117-39-5	0.09
Quercetin 3-(3-p-coumaroylglucoside)	4.653	610.1301	76211-70-6	0.03
Rhamnetin	5.528	316.0572	480-19-3	2.23
Taxifolin	4.405	304.0572	480-18-2	0.05
Cyanidin 3-O-rutinoside	4.334	594.1558	28338-59-2	9.62
Diosmetin	5.179	300.0621	520-34-3	0.95
Eriodictyol	4.51	288.0621	552-58-9	0.09
Genistein	4.478	270.0516	446-72-0	3.98
Genistin	4.476	432.1037	529-59-9	1.52
Luteolin	4.806	286.0465	491-70-3	2.03
Pelargonidin 3-O-(6-O-malonyl-β-D-glucoside)	4.525	518.1035	165070-68-8	0.04
Pelargonidin 3-O-rutinoside	4.389	578.1612	NA	0.05
Petunidin 3-O-glucoside	4.537	478.1092	6988-81-4	0.05
Quercitrin	4.503	448.0987	522-12-3	0.53
Sakuranin	4.532	448.1351	NA	0.06
Scutellarein 5-glucuronide	4.501	462.0778	NA	5.96
Naringin	4.482	580.1763	10236-47-2	0.02
Gallocatechin	1.388	306.0707	NA	0.10
Peonidin 3-rhamnoside 5-glucoside	13.76	609.1748	53859-11-3	0.08
Hesperetin	4.538	302.0778	520-33-2	0.13
2-Hexyl-3-phenyl-2-propenal	5.773	216.1506	101-86-0	20.99
DL-pipecolic acid	1.925	129.0785	535-75-1	1.21
Hydroquinidine	4.963	326.1984	1435-55-8	0.02
Hypoxanthine	1.963	136.0379	68-94-0	1.48
Trigonelline	1.584	137.0471	535-83-1	11.84
Xanthosine	4.474	284.0787	146-80-5	0.11
Caffeine	4.413	194.0837	58-08-2	0.07
D-Mannitol	1.231	182.0785	69-65-8	0.18
a-L-Rhamnose	1.239	164.0679	6014-42-2	0.08
Gibberellin A53	5.402	348.1923	NA	0.12
Glutinosone	5.699	220.1455	55051-94-0	13.78
Plaunol B	4.789	356.1247	69749-00-4	1.01
Quillaic acid	6.58	486.3329	631-01-6	0.03
Genipin	4.406	226.083	6902-77-8	0.34
Medicagenic acid	6.215	502.327	599-07-5	0.08
p-Cymene	4.894	134.1089	NA	0.18

Pantothenic Acid	3.524	219.1103	137-08-6	10.65
Pyridoxine	2.326	169.0736	65-23-6	1.34
Pyridoxal	3.258	167.0579	66-72-8	0.08
Niacin	5.633	123.0314	59-67-6	0.04
Niacinamide	1.985	122.0473	98-92-0	1.87
Palmitic amide	9.57	255.2558	629-54-9	1.77
13Z-Docosenamide	13.06	337.3334	112-84-5	12.71
Oleamide	9.873	281.2709	301-02-0	4.09
Stearamide	12.982	283.2865	124-26-5	1.02
Coumarin	5.111	146.0362	91-64-5	0.13
3 Hydroxycoumarin	3.902	162.0309	939-19-5	1.08
Scopoletin	4.766	192.0414	NA	0.25
Benzoic acid	4.7	122.0362	65-85-0	0.59
α-ketoisovaleric acid	1.86	116.0469	759-05-7	0.70
Succinic acid	1.957	118.0273	110-15-6	5.02
nandrolone	5.468	274.1923	434-22-0	1.10
α-Linolenic Acid	7.357	278.224	463-40-1	3.14
Butyric acid	1.866	88.0521	107-92-6	2.91
LysoPC(16:0)	7.257	495.3313	NA	0.95
MG(0:0/18:3/0:0)	6.214	352.2602	NA	0.09
Indoleacrylic acid	4.278	187.0625	1204-06-4	2.79
Methyl cinnamate	3.805	162.0675	103-26-4	0.26
5-Hydroxy-L-tryptophan	2.276	220.0845	4350-09-8	0.26
Indoleacetaldehyde	2.371	159.0681	NA	0.05
Acetylcholine	2.005	145.1099	51-84-3	3.80
Cinnamic acid	3.612	148.0521	621-82-9	0.22
Gingerol	5.765	294.182	58253-27-3	1.39
Hippuric acid	4.356	179.0576	495-69-2	0.10
Jasmolone	5.898	180.1144	54383-66-3	1.12
(-)-Jasmonic acid	5.713	210.1247	6894-38-8	10.95
Indole	4.301	117.0573	120-72-9	20.21
Methyl jasmonate	4.519	224.1403	39924-52-2	7.52
Phenylacetic acid	4.746	136.0518	103-82-2	0.81
acetophenone	4.403	120.0568	98-86-2	0.44
Choline	9.289	103.0991	62-49-7	0.03
Tropic acid	4.458	166.065	552-63-6	0.60

Table 2 Chemical components identified from AR by high-performance liquid chromatography-electrospray ionization/mass spectrometry (ESI -)

Name	Rt [min]	Molecular Weight	CAS	Content (ng/μL)
L-Isoleucine	2.06	131.09469	61-90-5	34.52
L-Phenylalanine	2.933	165.07893	63-91-2	211.45
Pyroglutamic acid	1.991	129.04272	98-79-3	401.32
L-Cystine	4.179	240.02653	56-89-3	5.94
Chlorogenic Acid	4.127	354.09478	327-97-9	1.41
ferulic acid	4.705	194.0574	1135-24-6	26.94
Sinapic acid	4.68	224.06787	530-59-6	11.20
1,2,3-Trihydroxybenzene	3.154	126.03172	533-73-3	8.90
Caffeic Acid	3.013	180.04208	4607-41-4	3.41
Gallic acid	3.708	170.02138	149-91-7	6.94
Gentisic acid	3.623	154.0266	490-79-9	88.81
Shikimic acid	1.836	174.05273	138-59-0	2.73
Homogentisic acid	3.694	168.04204	451-13-8	209.40
m-Coumaric acid	4.65	164.04712	588-30-7	148.77
Syringic acid	2.887	198.05249	530-57-4	7.29
Salicylic acid	4.496	138.03141	69-72-7	132.00
Uridine	2.02	244.06907	58-96-8	22.44
Inosine	1.276	268.07889	58-63-9	33.93
IMP	4.452	348.04661	131-99-7	4.17
cAMP	1.971	329.05183	60-92-4	9.29
Diosmetin	5.179	300.06245	520-34-3	7.96
Genistein	4.566	270.05208	446-72-0	37.27
Malvidin	5.272	330.07307	643-84-5	2.78
Naringenin	5.185	272.06776	480-41-1	4.14
Quercetin	5.038	302.04179	117-39-5	3.87
Cyanidin 3-O-rutinoside	4.326	594.15626	28338-59-2	192.70
Isorhamnetin	4.948	316.05741	480-19-3	1.67
Luteolin	4.861	286.04682	491-70-3	45.32
Pelargonidin 3-O-rutinoside	4.944	578.16133	NA	0.98
Petunidin 3-O-glucoside	4.585	478.10942	6988-81-4	3.95
Quercitrin	4.555	448.09913	522-12-3	7.41
Dihydromyricetin	4.479	320.05192	27200-12-0	1.21
Eriodictyol	4.523	288.06209	552-58-9	0.94
Naringin	4.499	580.17667	10236-47-2	0.95
Quercetin 3-(3-p-coumaroylglucoside)	4.67	610.12941	76211-70-6	1.07
Quercetin 3-galactoside	4.519	464.09335	482-36-0	1.39
Scutellarein 5-glucuronide	4.502	462.07786	NA	63.58
Taxifolin	4.43	304.05702	480-18-2	1.27
Rutin	4.428	610.14931	153-18-4	1.61
Hesperetin	4.523	302.07789	520-33-2	1.59
Purine	1.299	120.04223	120-73-0	349.43
2-Furoic acid	1.439	112.01615	88-14-2	241.17
Caffeine	4.492	194.08423	58-08-2	1.85
D-Glucarate	1.543	210.03737	87-73-0	63.10
D-Glucuronic acid	1.264	194.04247	6556-12-3	45.47
Glutaric acid	1.311	132.04226	110-94-1	235.59
L-Xylulose	1.458	150.05294	527-50-4	44.41
D-Mannitol	1.265	182.07878	69-65-8	140.84
Gluconic acid	1.299	196.058	526-95-4	1538.85
α-D-Glucose	1.307	180.06317	492-62-6	990.57
α,α-Trehalose	1.738	342.1154	57-50-1	65.82
Raffinose	4.067	504.16731	512-69-6	1.87
Genipin	4.414	226.08368	6902-77-8	18.67
Gibberellin A12	8.093	332.19787	NA	1.67
Medicagenic acid	6.193	502.32825	599-07-5	11.66
Quillaic acid	6.564	486.33328	631-01-6	2.14
Rishitin	7.443	222.16141	18178-54-6	38.69
Gibberellin A17	4.924	378.1664	18411-79-5	3.45
Gibberellin A36	5.465	362.17181	NA	1.11
Ganoderic acid H	17.348	572.2945	98665-19-1	20.01
Geranyl diphosphate	4.391	314.06284	763-10-0	48.34
Pantothenic Acid	3.485	219.1103	137-08-6	383.90
Riboflavin	4.246	376.1359	83-88-5	22.96

Sulfuric acid	1.575	97.96744	7664-93-9	1453.79
Phosphoric acid	1.471	97.97696	7664-38-2	170.76
Benzoic acid	4.717	122.03673	65-85-0	79.39
Citric acid	1.446	192.02674	77-92-9	2694.59
Lactic acid	2.959	90.0318	50-21-5	15.36
Pyruvate	1.45	88.01615	127-17-3	92.66
Hexadecanedioic acid	5.656	286.21382	NA	15.38
Quinic acid	4.373	192.06302	77-95-2	14.95
Aconitic acid	2	174.0164	499-12-7	178.17
Itaconic acid	2.512	130.02669	97-65-4	283.47
Maleic acid	1.996	116.01102	110-16-7	272.96
Malic acid	1.879	134.02155	6915-15-7	1291.47
Oxoglutaric acid	1.487	146.02162	328-50-7	20.79
Succinic acid	2.072	118.02664	110-15-6	1453.94
Glyceric acid	1.354	106.02678	473-81-4	85.25
nandrolone	5.46	274.19264	434-22-0	1.28
α-Linolenic Acid	7.321	278.22397	463-40-1	164.66
LysoPC(15:0)	7.22	481.31539	NA	39.74
Traumatic Acid	5.273	228.13561	6402-36-4	49.42
acetophenone	4.646	120.05742	98-86-2	94.66
Citramalic acid	1.499	148.03727	2306-22-1	110.90
Mevalonic acid	3.028	148.07363	150-97-0	74.37
Phenylacetic acid	4.741	136.05243	103-82-2	24.37
(-)-Jasmonic acid	5.711	210.12533	6894-38-8	378.66
Malonic acid	1.474	104.0111	141-82-2	566.06
Xanthoxin	6.275	250.15644	8066-07-07	259.70
Gentisin	4.621	258.05214	437-50-3	5.05
Tropic acid	4.432	166.06257	552-63-6	5.88
Xanthoxic acid	9.992	266.15443	NA	7.21

Figures

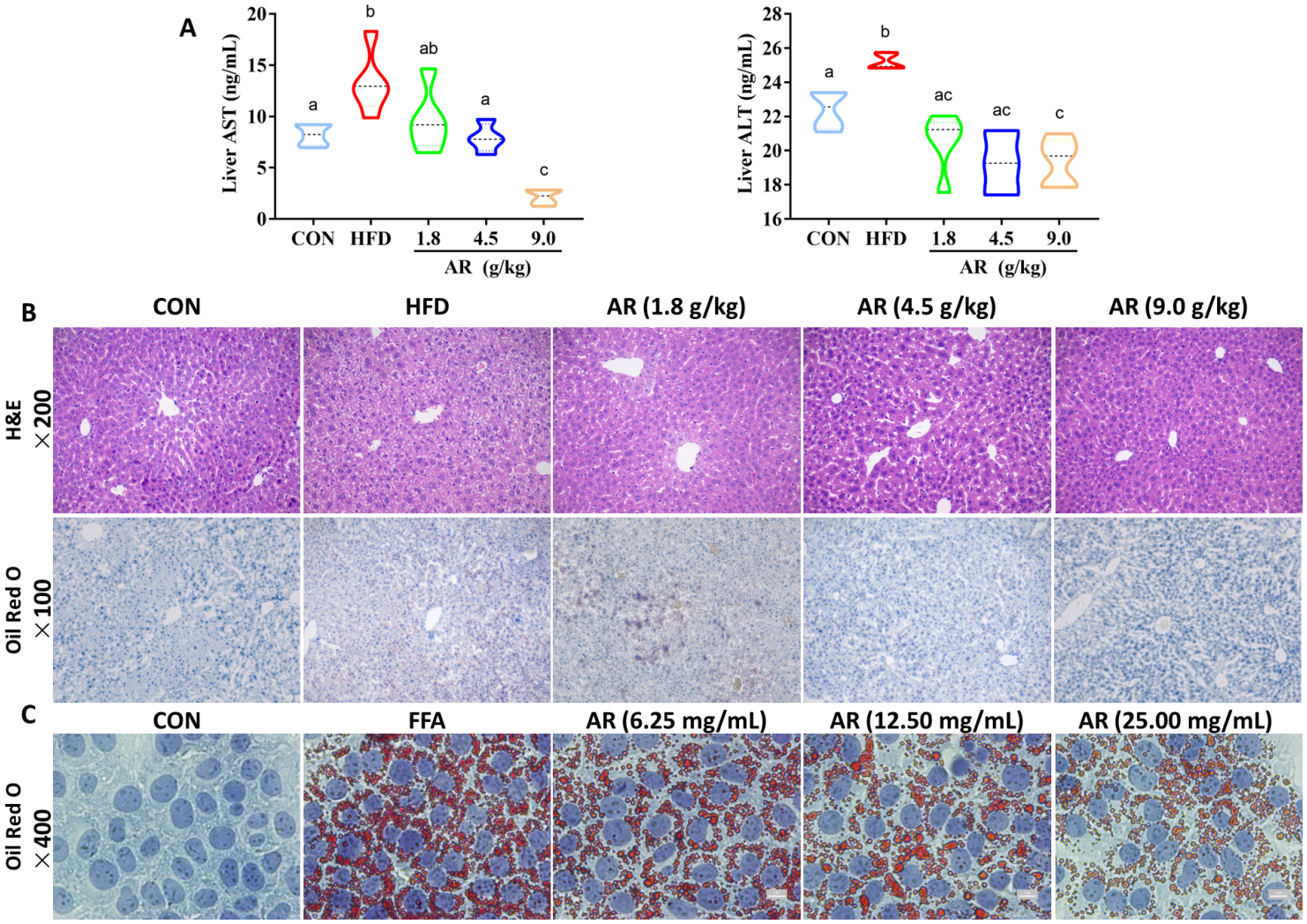

Figure 1

Effect of AR on liver histopathology of NAFLD induced by HFD. (A) The expression of alanine aminotransferase (ALT) and aspartate aminotransferase (AST) in liver. (B) H&E staining and Oil Red in liver. (C) Oil Red in AML12 cells. There are significant differences among the groups with different lowercase letters ($P < 0.05$). Groups: CON, control; HFD, high-fat diet; FFA, free fatty acid; AR, Agastache rugosa.

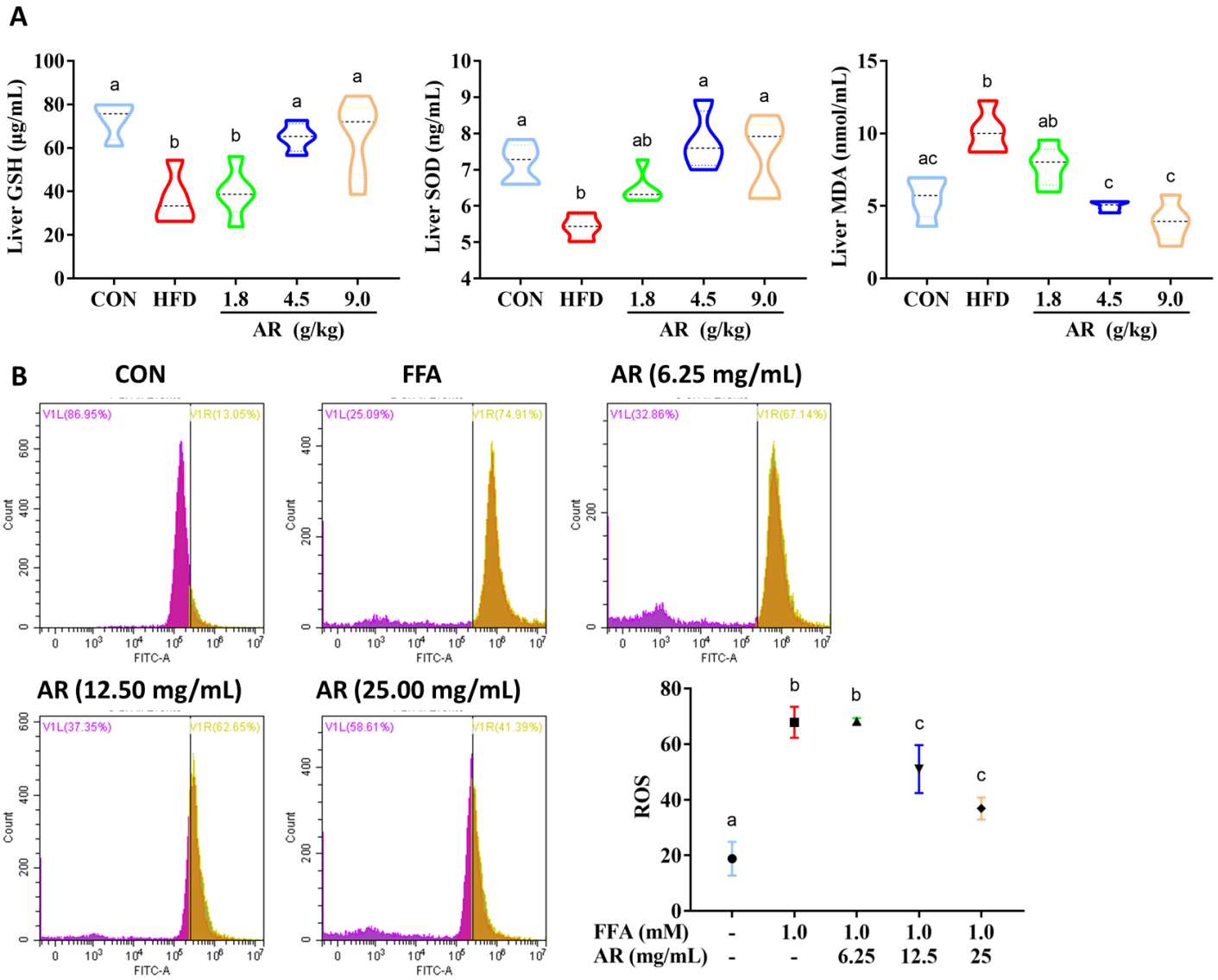

Figure 4

Effect of AR on oxidative stress in liver and AML12 cells. (A) The expression of glutathione (GSH), superoxide dismutase (SOD) and malondialdehyde (MDA) in liver. (B) Detection of ROS level in AML12 cells. There are significant differences among the groups with different lowercase letters ($P < 0.05$). Groups: CON, control; FFA, free fatty acid; AR, Agastache rugosa.

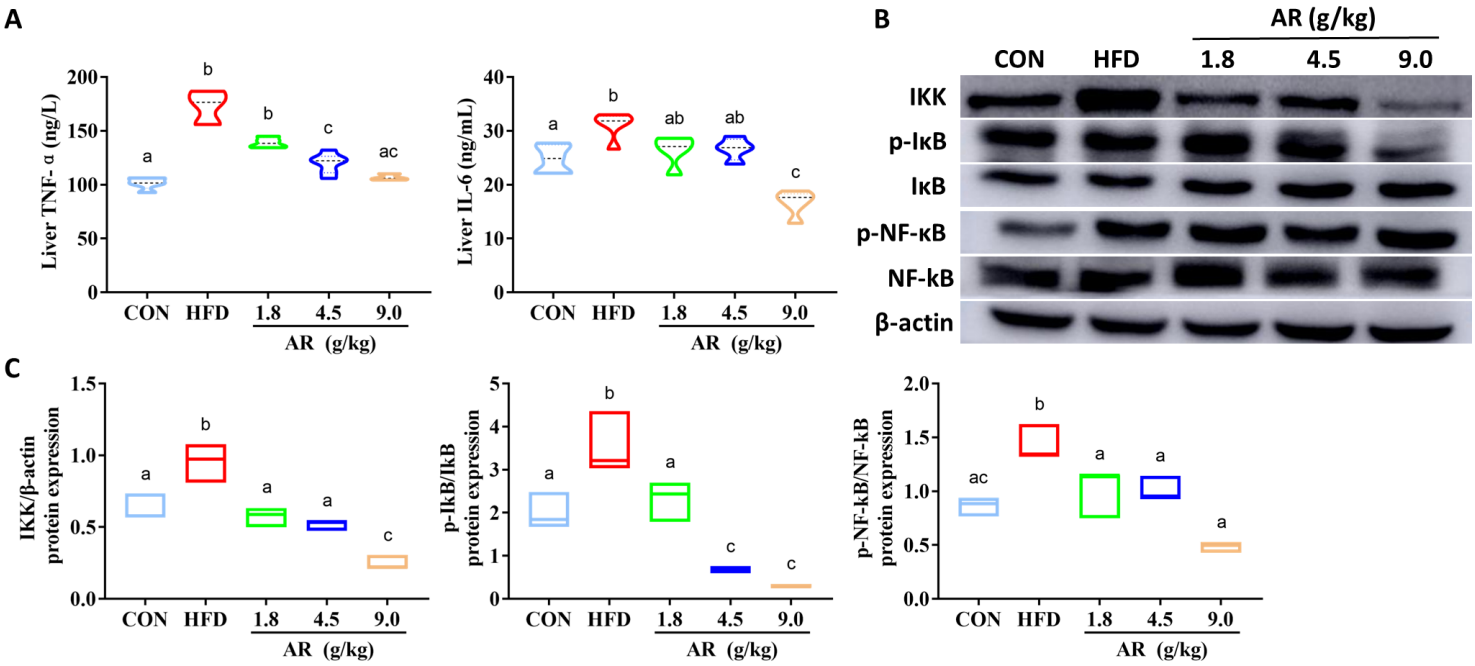

Figure 7

Effect of AR on hepatic inflammatory pathway of NAFLD induced by HFD. (A) Expression of tumor necrosis factor-α (TNF-α) and interleukin-6 (IL-6) in liver. (B) The expression of inhibitor of KappaB kinase (IKK), nuclear factor-κB (NF-κB), inhibitor of NF-κB (IκB), p-IκB and p-NF-κB protein in liver. (C) Quantitative analysis of Western blot density. There are significant differences among the groups with different lowercase letters ($P < 0.05$). Groups: CON, control; HFD, high-fat diet; AR, Agastache rugosa.

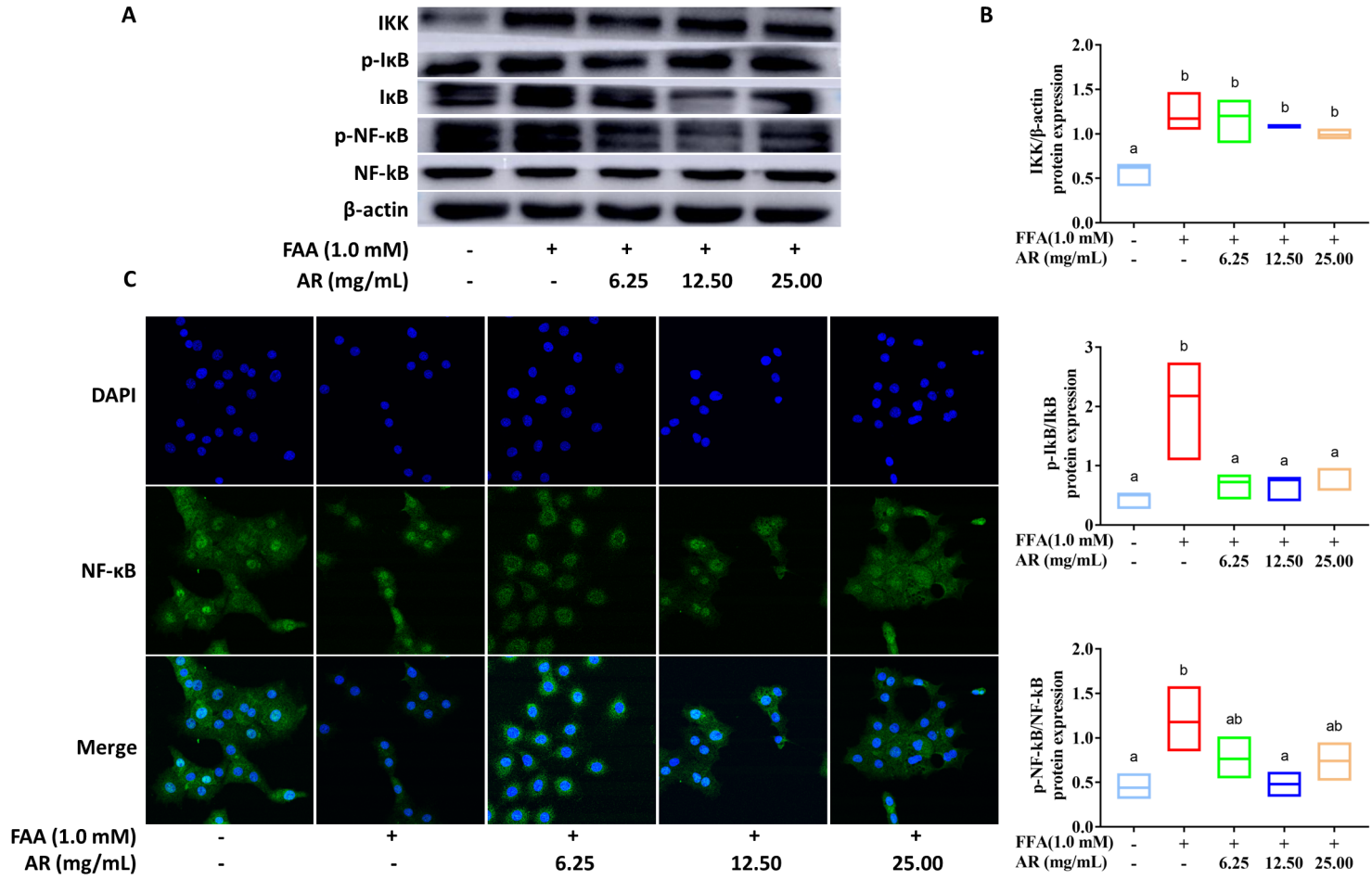

Figure 10

Effects of AR on AML12 cells inflammatory pathway. (A) The expression of KappaB kinase (IKK), nuclear factor-κB (NF-κB), inhibitor of NF-κB (IκBα), p-IκB and p-NF-κB protein in AML12 cells. (B) Quantitative analysis of Western blot density. (C) Detection of translocation of NF-κB. There are significant differences among the groups with different lowercase letters ($P < 0.05$). Groups: FFA, free fatty acid; AR, Agastache rugosa.

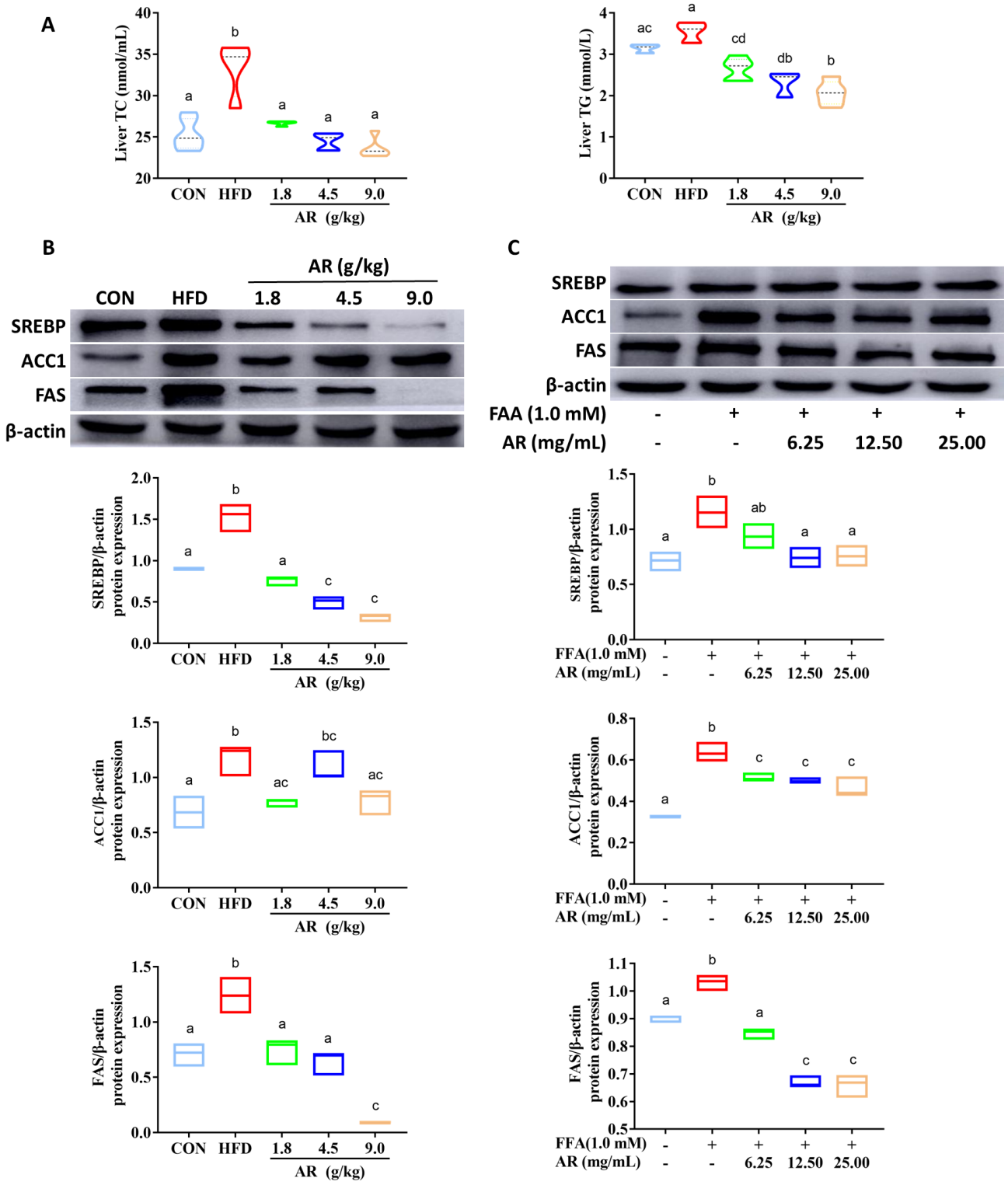

Figure 13

Effects of AR on liver andAML12 cells Lipid metabolism pathway. (A) Expression of total cholesterol (TC) and triglyceride (TG) in liver. (B) The expression of Lipid metabolism pathway protein in liver. (C) The expression of Lipid metabolism pathway protein in AML12 cells. There are significant differences among the groups with different lowercase letters ($P < 0.05$). SREBP: sterol regulatory element binding protein;

ACC1: acetyl-CoA carboxylase 1; FAS: fatty acid synthase. Groups: CON, control; HFD, high-fat diet; FFA, free fatty acid; AR, Agastache rugosa.

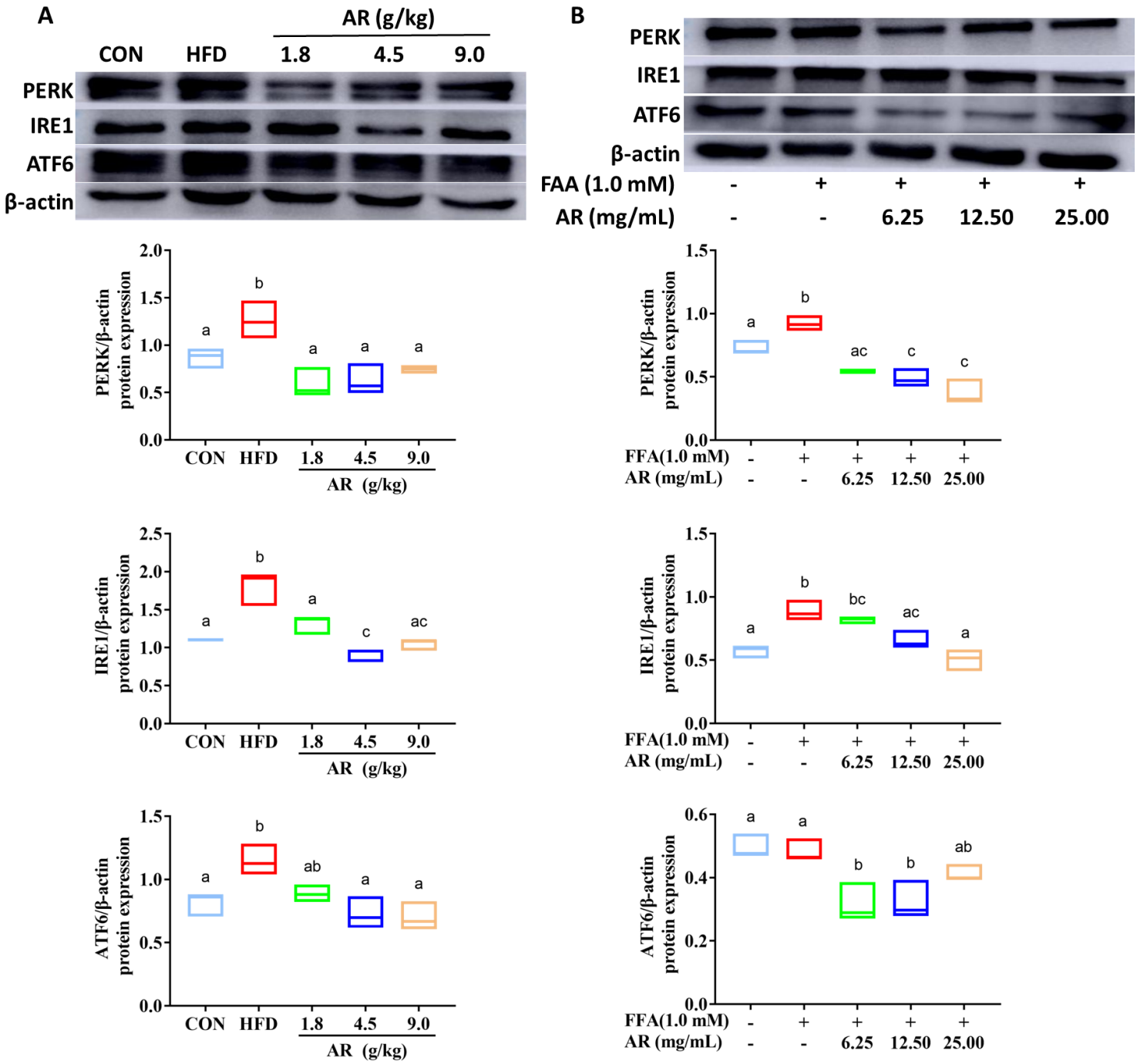

Figure 16

Effects of AR on ERS (endoplasmic reticulum stress) in liver andAML12 cells Lipid metabolism pathway. (A) The expression of protein kinase (PKR)-like endoplasmic reticulum kinase (PERK), inositol-requiring enzyme-1 (IRE1) and activating transcription factor 6 (ATF6) proteins in liver. (B) The expression of PERK, IRE1 and ATF6 protein in AML12 cells. There are significant differences among the groups with different lowercase letters ($P < 0.05$). Groups: CON, control; HFD, high-fat diet; FFA, free fatty acid; AR, Agastache rugosa.

Agastache rugosa

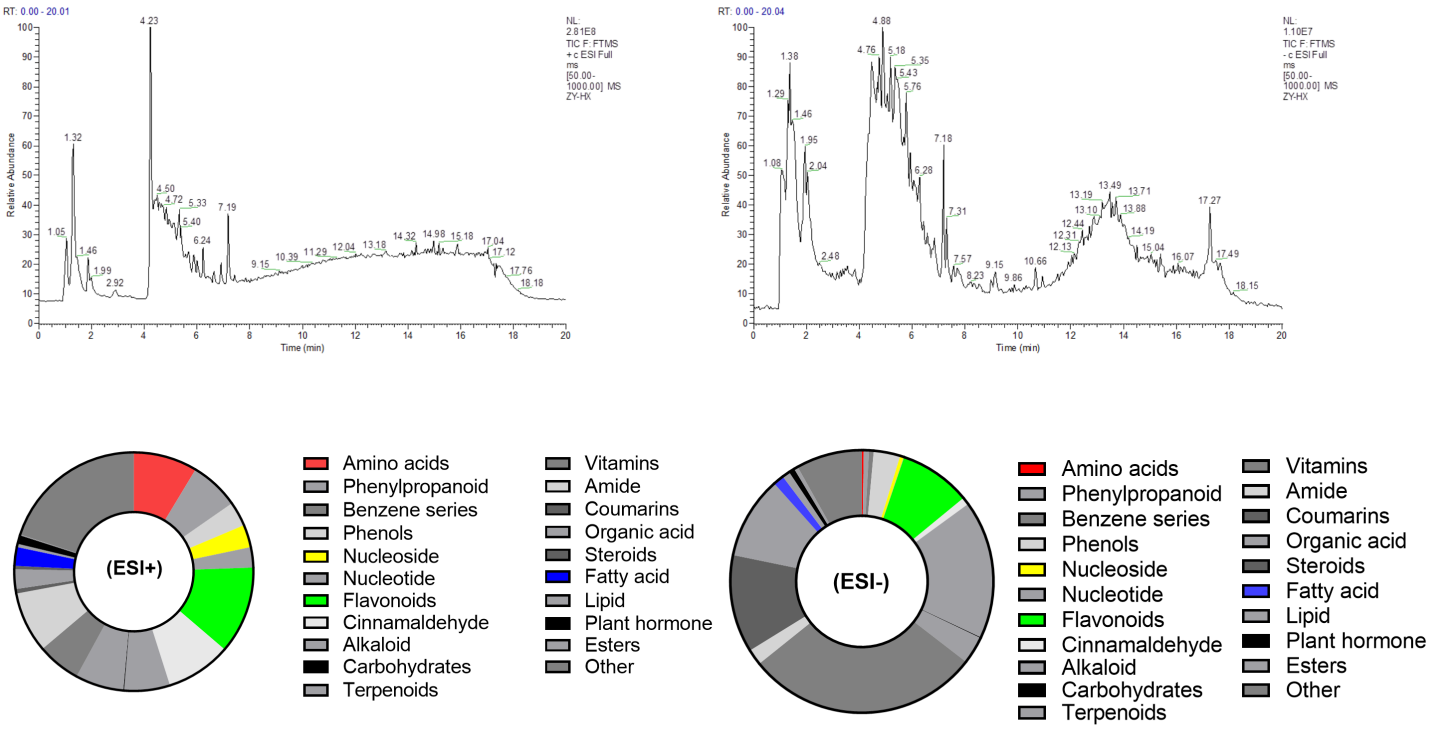

Figure 19

The Total Ion Chromatogram of AR. (ESI+) represents the positive ion detection mode, in which the mass analyzer scans only positive charged ions and filters out negative charged ions to obtain positive charged ions information during the detection process; (ESI-) denotes the negative ion detection mode, in which the mass analyzer scans only negative charged ions and filters out positive charged ions, thus obtaining the information of negative charged ions.